

Miniature UAV Empowered Reconfigurable Energy Harvesting Holographic Surfaces in THz Cooperative Networks

Yifei Song*[§], Jalal Jalali^{†§}, Filip Lemic[‡], Natasha Devroye^{‡‡}, and Jeroen Famaey[†]

*Bradley Department of Electrical and Computer Engineering, Virginia Tech, Blacksburg, VA 24060 USA

[†]IDLab, University of Antwerp - imec, Sint-Pietersvliet 7, 2000 Antwerp, Belgium

[§]Wireless Communication Research Group, JuliaSpace Inc., Chicago, IL, USA

[‡]AI-Driven Systems Lab, i2Cat Foundation, Spain

^{‡‡}University of Illinois Chicago, Chicago, IL, USA

Email: josh@juliaspace.com

Abstract—This paper focuses on enhancing the energy efficiency (EE) of a cooperative network featuring a ‘miniature’ unmanned aerial vehicle (UAV) that operates at terahertz (THz) frequencies, utilizing holographic surfaces to improve the network’s performance. Unlike traditional reconfigurable intelligent surfaces (RIS) that are typically used as passive relays to adjust signal reflections, this work introduces a novel concept: Energy harvesting (EH) using reconfigurable holographic surfaces (RHS) mounted on the miniature UAV. In this system, a source node facilitates the simultaneous reception of information and energy signals by the UAV, with the harvested energy from the RHS being used by the UAV to transmit data to a specific destination. The EE optimization involves adjusting non-orthogonal multiple access (NOMA) power coefficients and the UAV’s flight path, considering the peculiarities of the THz channel. The optimization problem is solved in two steps. Initially, the trajectory is refined using a successive convex approximation (SCA) method, followed by the adjustment of NOMA power coefficients through a quadratic transform technique. The effectiveness of the proposed algorithm is demonstrated through simulations, showing superior results when compared to baseline methods.

Index Terms—Cooperative communication, energy efficiency (EE), energy harvesting (EH), reconfigurable holographic surfaces (RHS), and miniature unmanned aerial vehicles (UAV).

I. INTRODUCTION

BUILDING on the original vision of 5G and extending into 6G, future wireless networks are expected to support massive machine-type communication (mMTC) with the requirements of improving scalability, resource efficiency, reducing latency, and minimizing energy consumption [1]. Researchers are investigating new network topologies focusing on establishing extensive backhaul links to boost network capacity [2]. Unmanned aerial vehicles (UAVs) have gained significant attention due to their unique advantage of establishing line-of-sight (LOS) communication links, enabling them to provide services to ground users while meeting quality of service (QoS) requirements. Specifically, miniature UAVs [3], such as nano-UAVs — distinguished by their palm-sized dimensions and weighing only a few tens of grams — are particularly well-suited for operations in confined spaces, thanks to their exceptional agility and compact design [4], [5]. Moreover, unlike standard-sized UAVs, miniature UAVs can safely operate in close proximity to humans [3], making them ideal for indoor applications. These capabilities open up possibilities for advanced applications, including surveillance, precise environmental monitoring, emergency search-and-rescue in collapsed structures, and enhanced immersive

virtual reality experiences through real-time mapping and interaction.

Simultaneously, ensuring massive connectivity under the mMTC framework presents a challenge, as accommodating trillions of devices within the congested and limited sub-6 GHz spectrum is increasingly difficult. To address this, a shift towards higher-frequency terahertz (THz) communication is being explored, offering data rates in the hundreds of Gbps [6]. Additionally, non-orthogonal multiple access (NOMA) [2] is gaining traction as a method to support multiple users simultaneously on the same frequency and time slots, using efficient interference cancellation techniques. Together, these advancements aim to meet the growing demands of next-generation communication networks.

More recently, the integration of UAVs with reconfigurable intelligent surfaces (RIS) has emerged as a promising approach to enhance wireless communication by utilizing the high mobility of UAVs and the ability of RIS to control signal reflections [7]. RIS technology, typically used as passive relays, adjusts the phase of incoming signals to improve coverage and capacity without requiring active amplification. However, *this paper focuses on a different concept: Energy Harvesting (EH) using Reconfigurable Holographic Surfaces (RHS)* [8], introducing a new aspect to RIS. We are the first to propose RHS as ultra-thin, lightweight surface antennas that go beyond conventional RIS, not only controlling signal reflections but also incorporating intelligent EH capabilities to directly power a network component, specifically a miniature UAV in our case. RHS offers unique advantages for UAV integration due to its compact design and low power consumption [9]. Moreover, since UAVs are typically constrained by limited battery capacity and must manage both communication and movement, energy efficiency (EE) becomes a critical concern. In this context, RHS significantly enhances the EE of UAV networks by harvesting energy from the impinging signals, thereby reducing the reliance on external power sources. This EH capability, combined with optimizing flight paths and improving communication quality of service (QoS), is crucial for maximizing the overall EE of THz UAV-assisted networks empowered by RHS.

To address this, some studies have proposed energy-aware UAV-RIS models to enhance the number of tasks completed per flight [10]. For example, in [11], the authors present an EE maximization problem and employ deep reinforcement

learning to optimize UAV power allocation and the RIS phase shift matrix. In [12], the authors introduced a solar-powered UAV-mounted RIS that provides external propulsion power and maximizes EE by optimizing the UAV trajectory alongside the beamforming active states. In [13], the authors studied a harvest-and-reflect (HaR) protocol designed to harvest energy for information transmission. In [14], the authors explored a hybrid access point that transfers energy to both the RIS and users, enabling self-sustainable information transmission following the energy harvesting (EH) process. There are also inherent challenges when considering the use of THz for EH in UAV-RHS systems. From a materials science perspective [15], THz waves are readily absorbed by materials, particularly biological substances that resonate at THz frequencies. This effect is especially significant in polar molecules, e.g., water, where THz radiation induces dipole moments, enhancing absorption. Consequently, the high absorptivity of THz waves poses challenges for their use in wireless communication¹.

Although there have been advancements [11]–[14], previous studies have not specifically explored the use of holographic surfaces solely for EH. In this paper, we harness the absorptive properties of the THz spectrum by equipping a miniature UAV with RHS for EH. This strategy extends battery life during data transmission and introduces a novel cooperative communication framework for air-to-ground transmission. The key contributions are as follows:

- To the best of our knowledge, this is the first work to use holographic surfaces purely for EH with no signal reflection alongside a novel THz NOMA cooperative communication model. In this model, a source node transmits: (1) a superimposed message to both the UAV and a destination node, utilizing different power coefficients in NOMA; and (2) a power signal to the RHS for EH, thereby prolonging its battery life.
- An optimization problem is formulated and solved to optimize the NOMA power allocation coefficients and the UAV trajectory in a three-dimensional (3D) system, aiming to maximize both the system's EE and the target transmission rate.

The paper is organized as follows: Section II presents the system model and optimization problem. Section III covers the solution approach. Section IV discusses simulation results, and Section V concludes with future research directions.

II. SYSTEM MODEL AND PROBLEM FORMULATION

We study a downlink NOMA transmission scenario with a miniature UAV-supported RHS cooperative framework. In Fig. 1, the source node communicates with two terminals: a miniature UAV and a receiver destination node. The UAV serves as an EH-RHS to guarantee the high rate requirement of the destination node. A 3D coordinate system is utilized, where the source and destination are positioned at $\mathbf{s}(t) =$

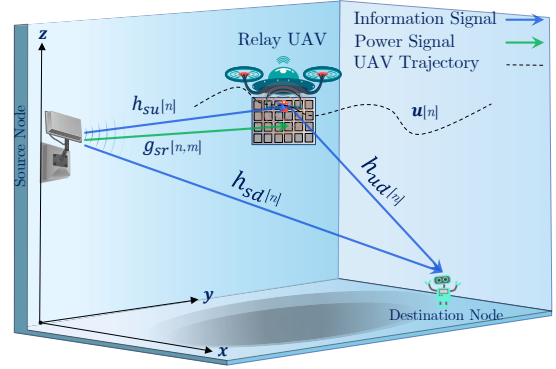


Fig. 1: Miniature UAV cooperative THz network empowered by EH RHS.

$[s_x(t), s_y(t), H_s]^T \in \mathbb{R}^{3 \times 1}$ and $\mathbf{d}(t) = [d_x(t), d_y(t), H_d]^T \in \mathbb{R}^{3 \times 1}$, respectively, with $[\cdot]^T$ as the transpose operation. The destination node remains static on the ground, while the UAV with RHS and the source maintain fixed altitudes, though they differ from one another, i.e., $H_u = H_r$ and H_s . At any given time $0 < t < T$, the UAV's instantaneous position is represented as $\mathbf{u}(t) = [x(t), y(t), H_u]^T \in \mathbb{R}^{3 \times 1}$. Moreover, the coordinates of the RHS-equipped UAV are expressed by $\mathbf{r}(t, m) = [x(t, m), y(t, m), H_u]^T \in \mathbb{R}^{3 \times 1}$, where $m = \{1, \dots, M\}$ refers to the index of each holographic element. The total flight time of the UAV, denoted as T , is divided into N equal time slots, with the trajectory at each time slot denoted as $\mathbf{u}[n], \forall n \in \{1, \dots, N\}$. Each slot is small enough to treat the UAV position as nearly constant. The UAV's position and speed are subject to the following constraints:

$$\mathbf{u}[1] = \mathbf{u}_s, \quad (1a)$$

$$\mathbf{u}[N+1] = \mathbf{u}_e, \quad (1b)$$

$$\|\mathbf{u}[n+1] - \mathbf{u}[n]\| \leq \Delta_t V_{\max}, \quad \forall n, \quad (1c)$$

where V_{\max} is the maximum allowable speed, Δ_t denotes the length of each time slot, and \mathbf{u}_s and \mathbf{u}_e represent the UAV's starting and ending positions, respectively. The channel coefficients for source-to-UAV and UAV-to-destination are $h_{su}[n]$ and $h_{ud}[n]$, which adhere to the free-space path loss model and are expressed as:

$$h_{su}[n] = \frac{g_0}{\|\mathbf{u}[n] - \mathbf{s}[n]\|} e^{-\frac{\xi(f)}{2} \|\mathbf{u}[n] - \mathbf{s}[n]\|}, \quad \forall n, \quad (2)$$

$$h_{ud}[n] = \frac{g_0}{\|\mathbf{u}[n] - \mathbf{d}[n]\|} e^{-\frac{\xi(f)}{2} \|\mathbf{u}[n] - \mathbf{d}[n]\|}, \quad \forall n, \quad (3)$$

and the channel gain between the source-to-RHS is given by:

$$g_{sr}[n, m] = \frac{g_0}{\|\mathbf{r}[n, m] - \mathbf{s}[n]\|} e^{-\frac{\xi(f)}{2} \|\mathbf{r}[n, m] - \mathbf{s}[n]\|}, \quad \forall n, m. \quad (4)$$

The THz path loss is represented by the exponential term, where $\xi(f)$ is the molecular absorption coefficient, influenced by frequency f and water vapor concentration [16]. For simplicity, we denote it as ξ , fixing the f . The reference power gain $g_0 = c/4\pi f$, with c as the speed of light [16]. The channel power gain $h_{sd}[n]$ between the source and destination follows a similar structure as in (2) and (3) [17].

Cooperative communication occurs in two episodes. In the first episode, the miniature UAV does EH using RHS and decodes information from the source while the destination receives its data. In the second episode, the UAV serves as an aerial relay, re-transmitting the data to the destination using the harvested energy from the first episode.

¹We hypothesize that if RHS for EH at THz frequencies is developed in the future, it could be made from materials that leverage this absorptive property of THz waves to enhance EH efficiency. To our knowledge, this has not yet been done.

A. Episode One: Direct Transmission and EH with RHS

In this episode, the source sends information to both the miniature UAV and the destination node using power-domain NOMA. The UAV, equipped with an RHS, acts as an EH user in this episode. The radio frequency (RF) source transmitted signal is:

$$s[n] = \sqrt{\mathfrak{P}_1[n]}s_1[n] + \sqrt{\mathfrak{P}_2[n]}s_2[n], \forall n, \quad (5)$$

where $s_1[n]$ and $s_2[n]$ represent the symbols transmitted in each time slot, modeled as independent circularly symmetric complex Gaussian (CSCG) variables with zero mean and unit variance. Furthermore, $\sqrt{\mathfrak{P}_1[n]}$ and $\sqrt{\mathfrak{P}_2[n]}$ correspond to the power allocation coefficients for NOMA in the n -th time slot, subject to the following constraints:

$$\mathfrak{P}_1[n] + \mathfrak{P}_2[n] \leq \mathcal{P}_{\text{peak}}, \forall n, \quad (6a)$$

$$\frac{1}{N} \sum_{n=1}^N \mathfrak{P}_1[n] + \mathfrak{P}_2[n] \leq \mathcal{P}_{\text{max}}, \quad (6b)$$

where $\mathcal{P}_{\text{peak}}$ is the maximum power the source can transmit in any time slot, and \mathcal{P}_{max} is the total power constraint across all time slots. The signal received by the information decoding (ID) antenna and the absorptive EH RHS elements on the miniature UAV from the RF source can be expressed as:

$$y_{\text{ID}}^{(1)}[n] = \sqrt{\varsigma_1[n]}h_{su}[n]s[n] + z_1^{(1)}[n], \forall n, \quad (7)$$

$$y_{\text{EH}}^{(1)}[n] = \sqrt{\varsigma_2[n]} \sum_{m=1}^M g_{sr}[n, m] \mathring{a}[m] e^{j\omega[m]} s[n] + z_2^{(1)}[n], \forall n, \quad (8)$$

where $z_1^{(1)}[n] \sim \mathcal{N}(0, \epsilon_1^2)$ and $z_2^{(1)}[n] \sim \mathcal{N}(0, \epsilon_2^2)$ represent the CSCG noise at the UAV's ID antenna and the EH RHS, respectively. Besides, $0 < \varsigma_1[n], \varsigma_2[n] < 1$ are the received ID and EH power factors. The parameters $\mathring{a}[m]$ and $\omega[m]$ denote the absorption coefficient and phase shift applied by the m -th element of the RHS.

Remark 1: The absorption coefficients on the RHS are assumed to be uniform, i.e., $\mathring{a}[m] = \mathring{a}_M, \forall m$. Nonlinearity and hardware impairments are not considered in this analysis. Additionally, no phase shift optimization is performed at the RHS, with the phase shifts uniformly set as $\omega[m] = \omega_M, \forall m$.

The miniature UAV utilizes successive interference cancellation (SIC) to decode the incoming signals. Specifically, it first decodes the destination node's data and then subtracts it from the received signal to retrieve its own data. The signal-to-interference-plus-noise ratio (SINR) at the UAV for detecting $s_2[n]$ is given by:

$$\mathfrak{J}_{d \leftarrow u}^{(1)}[n] = \frac{\mathfrak{P}_2[n]|h_{su}[n]|^2}{\mathfrak{P}_1[n]|h_{su}[n]|^2 + \epsilon_1^2[n]/\varsigma_1[n]}, \forall n. \quad (9)$$

Next, the SINR for decoding the miniature UAV's own data is expressed as:

$$\mathfrak{J}_r^{(1)}[n] = \frac{\varsigma_1[n]\mathfrak{P}_1[n]|h_{su}[n]|^2}{\epsilon_1^2[n]}, \forall n. \quad (10)$$

Based on (7) and (8), the RF power harvested by the EH RHS of the miniature UAV, neglecting the noise power, can be expressed as [13]:

$$\mathcal{E}[n] = \eta \mathring{a}_M e^{2j\omega_M} \mathcal{T}[n] \varsigma_2[n] \left| \sum_{m=1}^M g_{sr}[n, m] \right|^2, \forall n, \quad (11)$$

where $\eta \in (0, 1]$ is the energy conversion efficiency, and

$\mathcal{T}[n]$ represents the transmission time fraction for the first episode within the n -th time slot, assuming equal transmission durations for both episodes. Therefore, the UAV's transmit power in the second episode, empowered by the EH RHS, can be written as:

$$\mathcal{P}_{\text{RHS}}[n] = \frac{\mathcal{E}[n]}{1 - \mathcal{T}[n]}, \forall n. \quad (12)$$

The received signal at the destination is given by:

$$y_d^{(1)}[n] = h_{sd}[n]s[n] + \varrho_1^{(1)}[n], \forall n, \quad (13)$$

where $\varrho_1^{(1)}[n] \sim \mathcal{N}(0, \epsilon_1^2[n])$ is the received noise at the destination node during the first episode. The SINR at the destination then becomes:

$$\mathfrak{J}_d^{(1)}[n] = \frac{\mathfrak{P}_2[n]|h_{sd}[n]|^2}{\mathfrak{P}_1[n]|h_{sd}[n]|^2 + \epsilon_1^2[n]}, \forall n. \quad (14)$$

B. Episode Two: Cooperative Transmission

In this episode, the UAV utilizes the power harvested by the RHS, (12), to relay the destination node's data. Consequently, the signal received at the destination node is:

$$y_d^{(2)}[n] = \sqrt{\mathcal{P}_{\text{RHS}}[n]}h_{ud}[n]s_2[n] + \varrho_2^{(2)}[n], \forall n, \quad (15)$$

where $\varrho_2^{(2)}[n] \sim \mathcal{N}(0, \epsilon_2^2[n])$ is the noise at the destination node. The corresponding SINR is given by:

$$\mathfrak{J}_d^{(2)}[n] = \frac{\eta \mathring{a}_M^2 e^{2j\omega_M} \varsigma_2[n] \left| \sum_{m=1}^M g_{sr}[n, m] \right|^2 |h_{ud}[n]|^2}{\epsilon_2^2[n]}, \forall n. \quad (16)$$

Finally, the destination node applies maximal ratio combining (MRC) to integrate the signals received in both episodes. The overall SINR can be expressed as:

$$\mathfrak{J}_d^{\text{MRC}}[n] = \mathfrak{J}_d^{(1)}[n] + \mathfrak{J}_d^{(2)}[n], \forall n. \quad (17)$$

C. Resource Allocation Problem Formulation

We begin by defining the network's EE as the ratio of the total sum rate to the total power consumed by the network. Mathematically, this is represented as $\eta_{EE}[n] = \frac{R_{\text{sum}}[n]}{\mathcal{P}_{\text{sum}}[n]}$, where $R_{\text{sum}}[n] = \log_2(1 + \mathfrak{J}_r^{(1)}[n]) + \log_2(1 + \mathfrak{J}_d^{\text{MRC}}[n])$. Assuming a constant power consumption for the miniature UAV's flight, \mathcal{P}_c , the total transmission power of the system can be written as: $\mathcal{P}_{\text{sum}}[n] = \mathfrak{P}_1[n] + \mathfrak{P}_2[n] + \mathcal{P}_c - \mathcal{P}_{\text{RHS}}[n]$. To maximize the EE by optimizing the NOMA power allocation coefficients and the UAV's trajectory, we formulate the following optimization problem:

$$\text{P}_1 : \max_{\mathfrak{P}_1[n], \mathfrak{P}_2[n], \mathbf{u}[n]} \sum_{n=1}^N \eta_{EE}[n] \quad (18)$$

$$\text{s.t.} : \frac{1}{N} \sum_{n=1}^N \mathcal{P}_{\text{RHS}}[n] \geq \frac{1}{N} \sum_{n=1}^N \mathcal{P}[n], \quad (18a)$$

$$\mathfrak{J}_{d \leftarrow u}^{(1)}[n] \geq \mathfrak{J}_{\text{min}}[n], \forall n, \quad (18b)$$

$$\mathfrak{J}_d^{\text{MRC}}[n] \geq \gamma_{\text{min}}[n], \forall n, \quad (18c)$$

$$\mathcal{P}[n] \geq 0, \forall n, (1a)-(1c), (6a), (6b). \quad (18d)$$

The constraint (18a) ensures that the power harvested by the EH RHS of the miniature UAV over all time slots is greater than the minimum required harvested power $\mathcal{P}[n] = \frac{\mathcal{E}[n]}{\mathcal{T}[n]}$ (where $\mathcal{P}[n] = \mathcal{P}_{\text{EH}}$, representing the harvested power). Constraint (18b) guarantees successful decoding of the destination node's data at the UAV, with the SINR exceeding the threshold

$\mathcal{J}_{\min}[n]$, while (18c) enforces that the destination node's SINR remains above the minimum requirement $\gamma_{\min}[n]$, where $\gamma_{\min} \geq \mathcal{J}_{\min}$. Finally, (18d) ensures that the UAV's transmitted power is feasible and non-negative.

III. A TWO-STEP SEQUENTIAL APPROACH TO SOLVING THE EE OPTIMIZATION PROBLEM

The optimization problem P_1 is NP-hard and non-convex due to the interdependence among the optimization variables. Additionally, the objective function in P_1 is a sum of ratios, which makes traditional Dinkelbach method approaches unsuitable [18]. To address this, we propose a two-step approach that separates the optimization process, allowing each variable to be optimized independently.

A. Step One: Optimizing EH RHS Miniature UAV Trajectory

In this step, the trajectory of the miniature UAV is optimized while the NOMA power allocation coefficients remain fixed. The sum rate function remains non-convex due to the coupling of the optimization variables. However, to address this, the non-linear fractional objective function is first transformed into a subtractive form [19].

Theorem [19]: Let $\mathbf{u}^*[n]$ be the optimal solution to P_1 . Then, given the existence of two vectors, $\boldsymbol{\alpha} = [\alpha_1^*, \dots, \alpha_N^*]^T$ and $\boldsymbol{\beta} = [\beta_1^*, \dots, \beta_N^*]^T$, the following optimization problem provides an optimal solution as follows:

$$\max_{\mathbf{u}[n]} \sum_{n=1}^N \alpha_n^* [R_{\text{sum}}[n] - \beta_n^* (\mathcal{P}_{\text{sum}}[n])]. \quad (19)$$

Moreover, $\mathbf{u}^*[n]$ must satisfy the following conditions:

$$R_{\text{sum}}^*[n] - \beta_n^* (\mathcal{P}_{\text{sum}}[n]) = 0, \forall n, \quad (20)$$

$$1 - \alpha_n^* (\mathcal{P}_{\text{sum}}[n]) = 0, \forall n. \quad (21)$$

The equivalent subtractive form in (19), using the additional parameters $\boldsymbol{\alpha}^*, \boldsymbol{\beta}^*$, shares the same optimal solution as P_1 for fixed values of $\mathfrak{P}_1[n]$ and $\mathfrak{P}_2[n]$. Specifically, problem (19) can be solved iteratively using a two-layer approach consisting of inner and outer layers. In the inner layer, (19) is solved with fixed values of $\boldsymbol{\alpha}$ and $\boldsymbol{\beta}$. Then, equations (20) and (21) are updated in the outer layer to find the optimal $\{\boldsymbol{\alpha}^*, \boldsymbol{\beta}^*\}$.

1) **Inner-layer:** Here, we optimize the trajectory based on the optimal NOMA power allocation coefficients as follows²:

$$P_3 : \max_{\mathbf{u}[n]} \sum_{n=1}^N \alpha_n^* [R_{\text{sum}}[n] - \beta_n^* (\mathcal{P}_{\text{sum}}[n])] \quad (22)$$

$$s.t. : \sum_{n=1}^N \frac{\delta_1 e^{-\xi(\|\mathbf{u}[n]-\mathbf{s}[n]\|)}}{\|\mathbf{u}[n]-\mathbf{s}[n]\|^2} \geq \sum_{n=1}^N \mathcal{P}[n], \quad (22a)$$

$$\frac{\mathfrak{P}_2[n]}{\mathfrak{P}_1[n] + \delta_2 \|\mathbf{u}[n]-\mathbf{s}[n]\| e^{\xi(\|\mathbf{u}[n]-\mathbf{s}[n]\|)}} \geq \mathcal{J}_{\min}[n], \forall n, \quad (22b)$$

$$\frac{\delta_1 \mathfrak{G}_0^2}{\varepsilon_2^2[n]} \cdot \frac{e^{-\xi(\|\mathbf{u}[n]-\mathbf{s}[n]\| + \|\mathbf{u}[n]-\mathbf{d}[n]\|)}}{\|\mathbf{u}[n]-\mathbf{s}[n]\|^2 \|\mathbf{u}[n]-\mathbf{d}[n]\|^2} \quad (22c)$$

$$+ \frac{\mathfrak{P}_2[n] |h_{sd}[n]|^2}{\mathfrak{P}_1[n] |h_{sd}[n]|^2 + \varepsilon_1^2[n]} \geq \gamma_{\min}[n], \forall n, (1a) - (1c), (18d),$$

²Without loss of generality and to simplify analysis, as shown in Fig. 1, we take the bottom-left element of the RHS as the reference point to represent the UAV's horizontal location, that is $\mathbf{r}[n, m] \simeq \mathbf{u}[n], \forall m$.

where $\delta_1 = \eta M \tilde{\mathfrak{a}}_M^2 e^{2j\omega_M} \varsigma_2[n] \mathfrak{G}_0^2$ and $\delta_2 = \frac{\varepsilon_1^2[n]}{\varsigma_1[n] \mathfrak{G}_0^2}$. The optimization problem P_3 remains non-convex. Therefore, P_3 is reformulated into an equivalent form by introducing slack optimization variables, $(a[n], b[n], c[n], d[n])$, as follows:

$$P_4 : \max_{\mathbf{u}[n], a[n], b[n], c[n], d[n]} \sum_{n=1}^N \alpha_n^* [R_{\text{sum}}[n] - \beta_n^* (\mathcal{P}_{\text{sum}}[n])] \quad (23)$$

$$s.t. : \sum_{n=1}^N \frac{\delta_2}{e^{c[n]}} \geq \sum_{n=1}^N \mathcal{P}[n], \quad (23a)$$

$$\frac{\mathfrak{P}_2[n]}{\mathfrak{P}_1[n] + \delta_2 e^{c[n]}} \geq \mathcal{J}_{\min}[n], \forall n, \quad (23b)$$

$$\frac{\mathfrak{P}_2[n] |h_{sd}[n]|^2}{\mathfrak{P}_1[n] |h_{sd}[n]|^2 + \varepsilon_1^2[n]} + \frac{\delta_1 \mathfrak{G}_0^2}{\varepsilon_2^2[n] e^{c[n]+d[n]}} \geq \gamma_{\min}[n], \forall n, \quad (23c)$$

$$a[n] \leq \frac{\|\mathbf{u}[n]-\mathbf{s}[n]\|^2}{e^{-\xi\|\mathbf{u}[n]-\mathbf{s}[n]\|}}, b[n] \leq \frac{\|\mathbf{u}[n]-\mathbf{d}[n]\|^2}{e^{-\xi\|\mathbf{u}[n]-\mathbf{d}[n]\|}}, \forall n, \quad (23d)$$

$$a[n] \leq e^{c[n]}, \quad b[n] \leq e^{d[n]}, \forall n, (1a) - (1c), (18d), \quad (23e)$$

where

$$R_{\text{sum}}[n] = \log_2 \left(1 + \frac{\delta_2 \mathfrak{P}_1[n]}{e^{c[n]}} \right) + \log_2 \left(1 + \mathcal{J}_d^{(1)}[n] + \left(\frac{\delta_1 \mathfrak{G}_0^2}{\varepsilon_2^2[n]} \cdot \frac{1}{e^{c[n]+d[n]}} \right) \right).$$

Using these transformations, the main objective function and constraints become convex but still intractable. Therefore, successive convex approximation (SCA) using first-order Taylor expansions is applied to approximate P_4 as convex functions. The first-order lower bounds are given by:

$$e^{c[n]} \geq e^{c^{(k)}[n]} (1 + c[n] - c^{(k)}[n]) \triangleq \tilde{e}^{c[n]}, \forall n, \quad (25)$$

$$e^{d[n]} \geq e^{d^{(k)}[n]} (1 + d[n] - d^{(k)}[n]) \triangleq \tilde{e}^{d[n]}, \forall n, \quad (26)$$

$$\frac{\|\mathbf{u}[n]-\mathbf{s}[n]\|^2}{e^{-\xi\|\mathbf{u}[n]-\mathbf{s}[n]\|}} \geq \frac{\|\mathbf{u}^{(k)}[n]-\mathbf{s}[n]\|^2}{e^{-\xi\|\mathbf{u}^{(k)}[n]-\mathbf{s}[n]\|}} + (2 + \xi\|\mathbf{u}^{(k)}[n]-\mathbf{s}[n]\|) \cdot \frac{(\mathbf{u}^{(k)}[n]-\mathbf{s}[n])^T (\mathbf{u}[n]-\mathbf{u}^{(k)}[n])}{e^{-\xi\|\mathbf{u}^{(k)}[n]-\mathbf{s}[n]\|}} \triangleq \frac{\|\tilde{\mathbf{u}}[n]-\mathbf{s}[n]\|^2}{e^{-\xi\|\tilde{\mathbf{u}}[n]-\mathbf{s}[n]\|}}, \forall n, \quad (27)$$

$$\frac{\|\mathbf{u}[n]-\mathbf{d}[n]\|^2}{e^{-\xi\|\mathbf{u}[n]-\mathbf{d}[n]\|}} \geq \frac{\|\mathbf{u}^{(k)}[n]-\mathbf{d}[n]\|^2}{e^{-\xi\|\mathbf{u}^{(k)}[n]-\mathbf{d}[n]\|}} + (2 + \xi\|\mathbf{u}^{(k)}[n]-\mathbf{d}[n]\|) \cdot \frac{(\mathbf{u}^{(k)}[n]-\mathbf{d}[n])^T (\mathbf{u}[n]-\mathbf{u}^{(k)}[n])}{e^{-\xi\|\mathbf{u}^{(k)}[n]-\mathbf{d}[n]\|}} \triangleq \frac{\|\tilde{\mathbf{u}}[n]-\mathbf{d}[n]\|^2}{e^{-\xi\|\tilde{\mathbf{u}}[n]-\mathbf{d}[n]\|}}, \forall n, \quad (28)$$

where $e^{c^{(k)}[n]}$ and $e^{d^{(k)}[n]}$ represent the Taylor expansion points at iteration k . With this transformation, P_4 's approximation becomes:

$$P_5 : \max_{\mathbf{u}[n], a[n], b[n], c[n], d[n]} \sum_{n=1}^N \alpha_n^* [\tilde{R}_{\text{sum}}[n] - \beta_n^* (\mathcal{P}_{\text{sum}}[n])] \quad (29)$$

$$s.t. : \sum_{n=1}^N \frac{\delta_1}{\tilde{e}^{c[n]}} \geq \sum_{n=1}^N \mathcal{P}[n], \quad (29a)$$

$$\frac{\mathfrak{P}_2[n]}{\mathfrak{P}_1[n] + \delta_2 \tilde{e}^{c[n]}} \geq \mathcal{J}_{\min}[n], \forall n \quad (29b)$$

$$\frac{\mathfrak{P}_2[n] |h_{sd}[n]|^2}{\mathfrak{P}_1[n] |h_{sd}[n]|^2 + \varepsilon_1^2[n]} + \frac{\delta_1 \mathfrak{G}_0^2}{\varepsilon_2^2[n] \tilde{e}^{c[n]+d[n]}} \geq \gamma_{\min}[n], \forall n, \quad (29c)$$

$$a[n] \leq \frac{\|\tilde{\mathbf{u}}[n]-\mathbf{s}[n]\|^2}{e^{-\xi\|\tilde{\mathbf{u}}[n]-\mathbf{s}[n]\|}}, b[n] \leq \frac{\|\tilde{\mathbf{u}}[n]-\mathbf{d}[n]\|^2}{e^{-\xi\|\tilde{\mathbf{u}}[n]-\mathbf{d}[n]\|}}, \forall n, \quad (29d)$$

$$a[n] \leq \tilde{e}^{c[n]}, \quad b[n] \leq \tilde{e}^{d[n]}, \forall n, (1a) - (1c), (18d), \quad (29e)$$

$$\begin{aligned}
L_3(\mathfrak{p}_1[n], \mathfrak{p}_2[n], \mathbf{a}, \mathbf{b}, \Upsilon, \mathbf{c}, \mathfrak{d}) &= \sum_{n=1}^N \varpi[n] \mathfrak{p}_{\text{sum}}^2[n] + \frac{1}{2\mathfrak{z}} \left[\left(\sum_{n=1}^N \mathbf{a}_n + \mathfrak{z} \left(\frac{\epsilon_1^2[n]}{\varsigma_1[n]} - \frac{\mathfrak{p}_2[n] |h_{su}[n]|^2}{\mathfrak{f}_{\min}[n]} + \mathfrak{p}_1[n] |h_{su}[n]|^2 \right) \right)^+ \right]^2 \\
&+ \sum_{n=1}^N \frac{1}{4\varpi[n] \hat{R}_{\text{sum}}^2[n]} + \left(\sum_{n=1}^N \mathbf{b}_n + \mathfrak{z} (\epsilon_1^2[n] \chi[n] - \mathfrak{p}_2[n] |h_{sd}[n]|^2 + \mathfrak{p}_1[n] |h_{sd}[n]|^2 \chi[n]) \right)^+ + \left(\sum_{n=1}^N \Upsilon_n + \mathfrak{z} (\mathfrak{p}_1[n] + \mathfrak{p}_2[n] - \mathfrak{p}_{\text{peak}}) \right)^+ \\
&+ \left(\mathbf{c}_n + \mathfrak{z} \left(\frac{1}{N} \sum_{n=1}^N \mathfrak{p}_1[n] + \mathfrak{p}_2[n] - \mathfrak{p}_{\text{max}} \right) \right)^+ + \left(\sum_{n=1}^N \mathfrak{d}_n - \mathfrak{z} \mathfrak{p}[n] \right)^+ - \left(\sum_{n=1}^N \mathbf{a}_n^2 + \mathbf{b}_n^2 + \Upsilon_n^2 + \mathbf{c}_n^2 + \mathfrak{d}_n^2 \right), \quad (40)
\end{aligned}$$

where $\tilde{R}_{\text{sum}}[n] = R_{\text{sum}}[n]|_{e^c[n]=\tilde{e}^c[n], e^d[n]=\tilde{e}^d[n]}$. Optimization solvers can be employed to find a solution for P_5 [18][20][21].

2) **Outer-layer:** The damped Newton method is applied to find the optimal values for $\{\alpha, \beta\}$. Let $\theta_n(\beta_n) = R_{\text{sum}}^*[n] - \beta_n^*(\mathfrak{p}_{\text{sum}}[n])$ and $\theta_{N+j}(\alpha_j) = 1 - \alpha_j^*(\mathfrak{p}_{\text{sum}}[j])$, $j \in \{1, \dots, N\}$. As shown in [22], the solution $\{\alpha^*, \beta^*\}$ is optimal if and only if $\theta(\alpha, \beta) = [\theta_1, \theta_2, \dots, \theta_{2N}]^T = 0$. The updated values of α^{i+1} and β^{i+1} can be computed by:

$$\alpha^{i+1} = \alpha^i + \vartheta^i \boldsymbol{\mu}_{N+1:2N}^i, \quad \beta^{i+1} = \beta^i + \vartheta^i \boldsymbol{\mu}_{1:N}^i, \quad (30)$$

where $\boldsymbol{\mu} = [\hat{\theta}(\alpha, \beta)]^{-1} \theta(\alpha, \beta)$ with $\hat{\theta}(\alpha, \beta)$ being the Jacobian matrix of $\theta(\alpha, \beta)$, and ϑ^i is the largest value of Π^m at iteration i satisfying:

$$(31)$$

$$\|\theta(\alpha^i + \Pi^m \boldsymbol{\mu}_{N+1:2N}^i, \beta^i + \Pi^m \boldsymbol{\mu}_{1:N}^i)\| \leq (1 - \wp \Pi^m) \|\theta(\alpha, \beta)\|,$$

where $m \in \{1, 2, \dots\}$, $\Pi^m \in (0, 1)$, and $\wp \in (0, 1)$.

B. Step two: Optimizing NOMA Power Allocation Coefficients

Consider the following sum-fraction optimization problem:

$$\min_{\Omega \in C} \sum_{j=1}^J \frac{\mathcal{A}_j(\Omega)}{\mathcal{B}_j(\Omega)}, \quad (32)$$

where J represents the total number of fractional terms, and Ω is the vector of optimization variables within the feasible domain C . It can be shown (32) is equivalent to:

$$\min_{\Omega \in C, \varpi_j > 0} \sum_{j=1}^J \varpi_j \mathcal{A}_j^2(\Omega) + \sum_{j=1}^J \frac{1}{4\varpi_j} \frac{1}{\mathcal{B}_j^2(\Omega)}. \quad (33)$$

The solution to both (32) and (33) is identical. It is worth noting that if $\mathcal{B}_j(\Omega)$ is concave and $\mathcal{A}_j(\Omega)$ is convex, then problem (33) becomes a convex quadratic problem for the given ϖ_j . Building on this, the convex problem (33) is solved for a given $\varpi_j = 1/2\mathcal{B}_j(\Omega)\mathcal{A}_j(\Omega)$, and the value of ϖ_j is updated in the next iteration. Thus, with a fixed UAV trajectory, problem P_1 can be rewritten in the following equivalent form:

$$\text{P}_6: \min_{\mathfrak{p}_1[n], \mathfrak{p}_2[n], \varpi[n] > 0} \sum_{n=1}^N \varpi[n] \mathfrak{p}_{\text{sum}}^2[n] + \sum_{n=1}^N \frac{1}{4\varpi[n]} \frac{1}{\hat{R}_{\text{sum}}^2[n]} \quad (34)$$

$$s.t.: \frac{\mathfrak{p}_2[n] |h_{su}[n]|^2}{\mathfrak{f}_{\min}[n]} - \mathfrak{p}_1[n] |h_{su}[n]|^2 \geq \frac{\epsilon_1^2[n]}{\varsigma_1[n]}, \forall n, \quad (34a)$$

$$\mathfrak{p}_2[n] |h_{sd}[n]|^2 - \mathfrak{p}_1[n] |h_{sd}[n]|^2 \chi[n] \geq \epsilon_1^2[n] \chi[n], \forall n, \quad (34b)$$

$$(6a), (6b), (18d),$$

where $\chi[n] = \gamma_{\min}[n] - \frac{\delta_1 \left| \sum_{m=1}^M g_{sr}[n, m] \right|^2 |h_{ud}[n]|^2}{M g_0^2 \epsilon_2^2[n]}$ and $\varpi[n] = \frac{1}{2\mathfrak{p}_{\text{sum}}^2[n] \hat{R}_{\text{sum}}^2[n]}$. It is evident that all constraints are linear and convex. However, the objective function remains non-convex due to the non-concave nature of the sum rate function. To address this, we apply the result from the following corollary [18].

Corollary 1: Let \mathcal{F} be a monotonically decreasing function of the ratio $\frac{\mathcal{C}_j(\mathcal{U})}{\mathcal{D}_j(\mathcal{U})}$. The optimization problem

$$\min_{\mathcal{U} \in C} \sum_{j=1}^J \mathcal{F}_j \left(\frac{\mathcal{C}_j(\mathcal{U})}{\mathcal{D}_j(\mathcal{U})} \right), \quad (35)$$

is equivalent to:

$$\min_{\mathcal{U} \in C, \lambda_j} \sum_{j=1}^J \mathcal{F}_j \left(2\lambda_j \sqrt{\mathcal{C}_j(\mathcal{U})} - \lambda_j^2 \mathcal{D}_j(\mathcal{U}) \right), \quad (36)$$

where λ_j is updated iteratively as: $\lambda_j = \frac{\sqrt{\mathcal{C}_j(\mathcal{U})}}{\mathcal{D}_j(\mathcal{U})}$.

By applying the result from Corollary 1, the second term in the objective function of P_6 can be rewritten as:

$$\min_{\mathfrak{p}_1[n], \mathfrak{p}_2[n], \lambda[n]} \sum_{n=1}^N \frac{1}{4\varpi[n]} \frac{1}{\hat{R}_{\text{sum}}^2[n]}, \quad (37)$$

where

$$\hat{R}_{\text{sum}}[n] = \log_2(1 + \mathfrak{f}_r^1[n]) + \log_2 \left(1 + \mathfrak{f}_d^2[n] \right) \quad (38)$$

$$+ 2\lambda[n] \sqrt{\mathfrak{p}_2[n] |h_{sd}[n]|^2} - \lambda^2[n] (\mathfrak{p}_1[n] |h_{sd}[n]|^2 + \epsilon_1^2[n]),$$

with $\lambda[n] = \frac{\sqrt{\mathfrak{p}_2[n] |h_{sd}[n]|^2}}{\mathfrak{p}_1[n] |h_{sd}[n]|^2 + \epsilon_1^2[n]}$. Here, $\hat{R}_{\text{sum}}[n]$ becomes bi-concave in terms of both the power allocation coefficients and $\lambda[n]$. Consequently, the multi-convex optimization problem is formulated as:

$$\text{P}_7: \min_{\mathfrak{p}_1[n], \varpi[n]} \sum_{n=1}^N \varpi[n] \mathfrak{p}_{\text{sum}}^2[n] + \sum_{n=1}^N \frac{1}{4\varpi[n]} \frac{1}{\hat{R}_{\text{sum}}^2[n]} \quad (39)$$

$$s.t.: (6a), (6b), (18d), (34a), (34b),$$

where $\mathfrak{I}[n] = [\mathfrak{p}_1[n], \mathfrak{p}_2[n]] \in \mathbb{R}^{2 \times 1}$. Note that $\mathfrak{p}_{\text{sum}}[n]$ depends on the power allocation coefficients, and each coefficient is subject to its respective constraints. Thus, $\mathfrak{p}_{\text{sum}}[n]$ and $\hat{R}_{\text{sum}}[n]$ are decoupled to enable the distributed optimization of $\mathfrak{p}_{\text{sum}}[n]$. To solve this, the augmented Lagrangian method (ALM) is applied, as defined in (40), where a penalty term is introduced in the Lagrange function of P_7 , yielding a sub-optimal solution. In (40), \mathfrak{z} represents the penalty factor, while $\mathbf{a}, \mathbf{b}, \Upsilon, \mathbf{c}, \mathfrak{d}$ are the Lagrange multipliers. Finally, the complexity of the proposed solution is determined by solving \mathfrak{p}_2 , \mathfrak{p}_5 , and \mathfrak{p}_7 , with complexities of $\mathcal{O}(9N^3)$, $\mathcal{O}((8N+3)(5N)^3)$, and $\mathcal{O}(N^2)$, respectively. Thus, the overall complexity of the proposed two-step method is approximately polynomial of degree four [18].

IV. SIMULATION RESULTS AND DISCUSSIONS

Our simulation setup involves a scenario within a square area, each side being 30 meters, containing one user and a miniature UAV, both randomly placed. To minimize path loss peaks, the carrier frequency is set to $f = 1.2$ THz with a transmission bandwidth of 10 GHz. The model also considers the frequency-dependent absorption coefficient, $\xi(f)$, which accounts for molecular absorption loss due to water vapor [23]. All statistical results are derived from aggregating

TABLE I: Simulation Parameters for EE Maximization of THz-NOMA Networks Empowered by Holographic Surfaces for Miniature UAVs.

Parameter	Value
Area side length	30 meters
Carrier frequency	1.2 THz
Transmission bandwidth	10 GHz
Absorption coefficient, $\xi(f)$	0.005
RHS absorption coefficient, $\hat{\alpha}_M$	1
Maximum miniature UAV flying speed, V_{\max}	1 meter/second
Duration of each time slot, Δ_t	0.1 second
Miniature UAV Operation time, T	45 second
Noise power spectral density	-174 dBm/Hz
Source Node altitude, H_s	2 meters
Miniature UAV altitude, H_u	3 meters
Peak power, p_{peak}	1 W
Circuit power, p_c	0.52 W

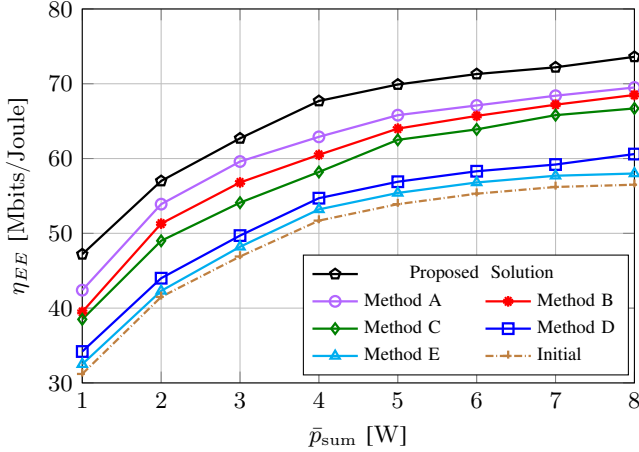


Fig. 2: The impact of average network transmit power, \bar{p}_{sum} , on the EE of THz-NOMA networks with a miniature UAV empowered by holographic surfaces data gathered through an extensive set of simulation trials, which include 1000 random realizations of channel gains. This systematic approach provides an in-depth understanding of the dynamics associated with deploying and operating the miniature UAV under specified environmental conditions, offering essential insights for optimizing UAV-assisted communication networks. A summary of all simulation parameters is presented in Table I [16], [24], [25].

To thoroughly assess the performance of our proposed resource allocation algorithm, we conducted a comparative study using the following benchmarks, each selected to highlight different system aspects:

- Method A: Assesses the algorithm’s performance within a fixed NOMA framework, providing a baseline for how the algorithm performs with static power coefficients.
- Method B: Compares NOMA and OMA to identify which access scheme is more efficient, crucial for understanding the benefits of multi-user communication in this context.
- Method C: Tests the algorithm with a fixed UAV flight path, isolating the effects of UAV trajectory optimization and measuring its contribution to overall performance.
- Method D: Evaluates a scenario without RHS, focusing on consistent power splitting EH at the UAV antenna. This shows the impact of RHS on EH and EE.
- Method E: Implements a fractional programming approach [26] without RHS for comparison, highlighting the benefits of incorporating RHS in our proposed solution.

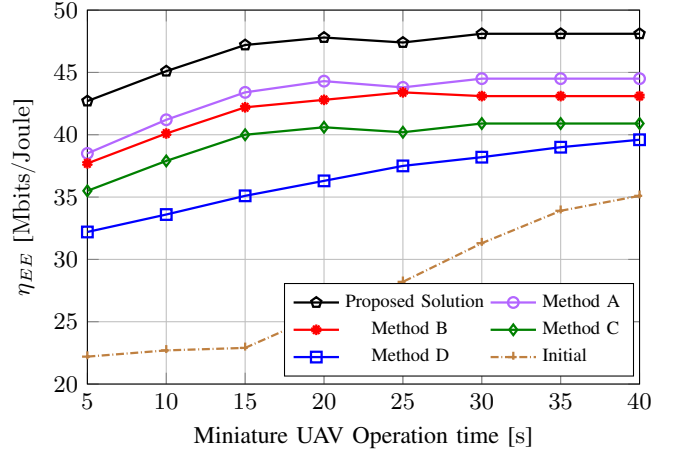


Fig. 3: The EE versus the operational time of the miniature UAV-empowered holographic surfaces in the THz-enabled network.

Fig. 2 illustrates the EE dynamics as influenced by the average network transmission power, expressed as $\bar{p}_{\text{sum}} = p_{\text{max}} + p_{\text{peak}} + p_c - p_{\text{EH}}$. In this figure, the ‘Initial’ curve depicts the EE performance based on an initial, unoptimized (random) configuration of the miniature UAV’s flight path. A key finding from our analysis is that our proposed algorithm consistently surpasses various benchmark methods, with its advantage becoming more evident as \bar{p}_{sum} increases, resulting in a widening performance gap. The results demonstrated the effectiveness of our proposed approach, showing improvements of: 30.3% over Method E, 23.0% over Method D, 21.2% over Method C, 18.1% over Method B, and 7.26% over Method A. These results strongly affirm the proposed algorithm’s ability to significantly boost EE, proving its effectiveness within miniature UAV-empowered RHS communication networks.

Fig. 3 offers a detailed examination of how the mission duration, represented by the miniature UAV’s operational time T , affects EE across various benchmark schemes. The analysis reveals an interesting pattern: as mission time increases, there’s a noticeable rise in EE for schemes utilizing fixed trajectories (Method D) and those starting with non-optimized but feasible configurations (‘Initial’). This improvement in EE is due to extended communication opportunities and the ability to adjust flight parameters over time. However, this trend is not consistent across all methods; specifically, Methods A, B, and C do not show the same EE increase as T grows. Quantitatively, extending the mission duration results in EE improvements of at least 37.1%, 26.8%, 22.8%, and 16.5%, 12.8%, respectively. These gains indicate that longer mission times provide a strategic benefit by allowing the holographic surfaces-assisted miniature UAV to optimize communication metrics and flight adjustments, enhancing overall network QoS. Nevertheless, the relationship between mission time and EE is complex. The interplay among optimization variables produces a non-linear, though generally increasing, trend in EE as mission duration extends. This highlights the intricate dynamics of EE optimization, where certain adjustments can lead to substantial gains. The observation that mission duration significantly impacts EE emphasizes an important challenge: *minimizing the task completion time for miniature UAV-empowered holographic*

surfaces relay systems while meeting specific EE targets. This requires balancing operational efficiency and mission urgency, suggesting a rich area for further research into optimizing UAV-based communication networks, with or without EH capabilities.

V. CONCLUSION AND FUTURE WORK

In this paper, we explored the complexities of improving the efficiency of a cooperative THz NOMA-based miniature UAV network powered by EH holographic surfaces. We began by formulating an EE optimization problem aimed at refining the network's resource allocation strategy. A novel deployment plan for the miniature UAV was introduced, designed to enhance THz wireless connectivity while accounting for molecular absorption effects, a crucial element in the path loss channel gain model for THz-enabled UAVs. Building on this, we developed an optimization framework to enhance EE, ensuring it met stringent QoS requirements. The optimization targeted key decision variables, including miniature UAV positioning and NOMA power allocation coefficients, based on a two-episode iterative solution. We demonstrated the effectiveness of the resource allocation algorithm through numerical results, highlighting its advantage when compared to baseline scenarios without trajectory and NOMA power optimizations. Our approach significantly improved network efficiency, extending UAV operational time and battery life, marking a major advancement in the capabilities of THz-NOMA miniature UAV networks with RHS. A potential direction for future research is to create a more realistic nonlinear EH model for RHS that incorporates active elements, enabling them to simultaneously *absorb* energy for harvesting and *reflect* signals for communication purposes. Another exciting area would be optimizing the phase shifters of RHS to improve the energy absorption capabilities of each surface and, therefore, maximize EH.

VI. ACKNOWLEDGMENTS

This work was supported by the Research Foundation - Flanders (FWO) project WaveVR (Grant number G034322N). It was also partially funded by the Spanish Ministry of Economic Affairs and Digital Transformation, along with the European Union — NextGeneration EU, under the framework of the Recovery, Transformation, and Resilience Plan (PRTR, Call UNICO I+D 5G 2021, ref. number TSI-063000-2021-7), as well as by the European Union's Horizon Europe research program under grant agreement n° 101139161 — INSTINCT project.

REFERENCES

- [1] S. Jere, Y. Song, Y. Yi, and L. Liu, "Distributed learning meets 6G: A communication and computing perspective," *IEEE Wirel. Commun.*, vol. 30, pp. 112–117, Feb. 2023.
- [2] M. Elbayoumi, M. Kamel, W. Hamouda, and A. Youssef, "NOMA-assisted machine-type communications in UDN: State-of-the-art and challenges," *IEEE Commun. Surv. Tutor.*, vol. 22, pp. 1276–1304, Mar. 2020.
- [3] K. Kalenberg, H. Müller, T. Polonelli, A. Schiaffino, V. Niculescu, C. Cioflan, M. Magno, and L. Benini, "Stargate: Multimodal sensor fusion for autonomous navigation on miniaturized UAVs," *IEEE Internet Things J.*, vol. 11, pp. 21372–21390, Jun. 2024.
- [4] N. Cheng, S. Wu, X. Wang, Z. Yin, C. Li, W. Chen, and F. Chen, "AI for UAV-assisted IoT applications: A comprehensive review," *IEEE Internet Things J.*, vol. 10, pp. 14438–14461, Aug. 2023.

- [5] M. F. Dehkordi and B. Jabbari, "Joint long-term processed task and communication delay optimization in UAV-assisted MEC systems using DQN," *arXiv preprint arXiv:2409.16102*, Sep. 2024.
- [6] J. Jalali, A. Khalili, H. Tabassum, R. Berkvens, J. Famaey, and W. Saad, "Energy-efficient THz NOMA for SWIPT-aided miniature UAV networks," *IEEE Commun. Lett.*, vol. 28, pp. 1107–1111, May 2024.
- [7] S. Hao, X. Fan, X. Li, L. Zhen, and J. Cui, "Uplink performance analysis of RIS-assisted UAV communication systems with random 3-D mobile pattern," *IEEE Internet Things J.*, vol. 11, pp. 28153–28168, May 2024.
- [8] R. Deng, B. Di, H. Zhang, H. V. Poor, and L. Song, "Holographic MIMO for LEO satellite communications aided by reconfigurable holographic surfaces," *IEEE J. Sel. Areas Commun.*, vol. 40, pp. 3071–3085, Oct. 2022.
- [9] R. Deng, B. Di, H. Zhang, D. Niyato, Z. Han, H. V. Poor, and L. Song, "Reconfigurable holographic surfaces for future wireless communications," *IEEE Wirel. Commun.*, vol. 28, pp. 126–131, Dec. 2021.
- [10] D. Tyrovolas, P.-V. Mekikis, S. A. Tegos, P. D. Diamantoulakis, C. K. Liaskos, and G. K. Karagiannidis, "Energy-aware design of UAV-mounted RIS networks for IoT data collection," *IEEE Trans. Commun.*, vol. 71, pp. 1168–1178, Feb. 2023.
- [11] K. K. Nguyen, S. R. Khosravirad, D. B. da Costa, L. D. Nguyen, and T. Q. Duong, "Reconfigurable intelligent surface-assisted multi-UAV networks: Efficient resource allocation with deep reinforcement learning," *IEEE J. Sel. Top. Signal Process.*, vol. 16, pp. 358–368, Apr. 2022.
- [12] Y. Xiao, D. Tyrovolas, S. A. Tegos, P. D. Diamantoulakis, Z. Ma, L. Hao, and G. K. Karagiannidis, "Solar powered UAV-mounted RIS networks," *IEEE Commun. Lett.*, vol. 27, pp. 1565–1569, Jun. 2023.
- [13] D. Tyrovolas, S. A. Tegos, V. K. Papanikolaou, Y. Xiao, P.-V. Mekikis, P. D. Diamantoulakis, S. Ioannidis, C. K. Liaskos, and G. K. Karagiannidis, "Zero-energy reconfigurable intelligent surfaces (zeRIS)," *IEEE Trans. Wirel. Commun.*, vol. 23, pp. 7013–7026, Jul. 2024.
- [14] B. Lyu, P. Ramezani, D. T. Hoang, S. Gong, Z. Yang, and A. Jamalipour, "Optimized energy and information relaying in self-sustainable IRS-empowered WPCN," *IEEE Trans. Commun.*, vol. 69, pp. 619–633, Jan. 2021.
- [15] S. Zhou *et al.*, "Patterned graphene-based metamaterials for terahertz wave absorption," *Coatings*, vol. 13, no. 1, p. 59, 2022.
- [16] Q. Li, A. Nayak, Y. Zhang, and F. R. Yu, "A cooperative recharging-transmission strategy in powered UAV-aided terahertz downlink networks," *IEEE Trans. Veh. Technol.*, vol. 72, pp. 5479–5484, Apr. 2023.
- [17] C. Chaccour, M. N. Soorki, W. Saad, M. Bennis, and P. Popovski, "Can terahertz provide high-rate reliable low-latency communications for wireless VR?," *IEEE Internet Things J.*, vol. 9, pp. 9712–9729, Jun. 2022.
- [18] J. Jalali, A. Khalili, A. Rezaei, R. Berkvens, M. Weyn, and J. Famaey, "IRS-based energy efficiency and admission control maximization for IoT users with short packet lengths," *IEEE Trans. Veh. Technol.*, vol. 72, pp. 12379–12384, Sep. 2023.
- [19] Y. Jong, *An efficient global optimization algorithm for nonlinear sum-of-ratios problem*. Center of Natural Science, University of Sciences, Pyongyang, DPR Korea, May 2012.
- [20] J. Jalali, *Resource allocation for SWIPT in multi-service wireless networks*. M.Sc. Thesis, Dept. Telecommun. Inf. Process., TELIN/IMEC, Ghent Univ., Ghent, Belgium, Jun. 2020 [Online]. Available: <https://arxiv.org/abs/2007.13676>.
- [21] J. Jalali, M. B. Madrid, F. Lemic, H. Tabassum, J. Struye, J. Famaey, and X. C. Perez, "Location optimization and resource allocation of IRS in a multi-user indoor mmWave VR network," in *2024 IEEE Wireless Commun. and Netw. Conf. (WCNC)*, pp. 1–6, 2024.
- [22] J. Jalali, A. Khalili, A. Rezaei, J. Famaey, and W. Saad, "Power-efficient antenna switching and beamforming design for multi-user SWIPT with non-linear energy harvesting," in *Proc. IEEE 20th Consumer Commun. Netw. Conf.*, pp. 746–751, Las Vegas, NV, USA, 2023.
- [23] J. M. Jornet and I. F. Akyildiz, "Channel modeling and capacity analysis for electromagnetic wireless nanonetworks in the terahertz band," *IEEE Trans. Wirel. Commun.*, vol. 10, pp. 3211–3221, Oct. 2011.
- [24] S. Yin, Y. Zhao, L. Li, and F. R. Yu, "UAV-assisted cooperative communications with power-splitting information and power transfer," *IEEE Trans. Green Commun. Netw.*, vol. 3, pp. 1044–1057, Dec. 2019.
- [25] J. Jalali, F. Lemic, H. Tabassum, R. Berkvens, and J. Famaey, "Toward energy efficient multiuser IRS-assisted URLLC systems: A novel rank relaxation method," in *2023 IEEE Globecom Workshops (GC Wkshps)*, pp. 1354–1360, 2023.
- [26] R. Zhang, R. Tang, Y. Xu, and X. Shen, "Resource allocation for UAV-assisted NOMA systems with dual connectivity," *IEEE Wirel. Commun. Lett.*, vol. 12, pp. 341–345, Feb. 2023.